J|A|C|S
ARTICLES
Published on Web 01/11/2007

The Mechanistically Significant Coordination Chemistry of Dinitrogen at FeMo-co, the Catalytic Site of Nitrogenase

Ian Dance

Contribution from the School of Chemistry, University of New South Wales, Sydney 2052, Australia

Received June 23, 2006; E-mail: i.dance@unsw.edu.au

Abstract: Reported here is a comprehensive theoretical investigation of the binding of N_2 to the Fe_7MoS_9N-(homocitrate)(cysteine)(histidine) active site (FeMo-co) of the enzyme nitrogenase, as a prerequisite to elucidation of the chemical mechanism of the catalyzed reduction to NH_3. The degree and type of hydrogenation of FeMo-co, with H atoms and possibly an H_2 molecule, are key variables, following the Thorneley−Lowe kinetic scheme. Ninety-four local energy minima were located for N_2 coordinated in η^2 (side) and η^1 (end) modes at the endo and exo coordination positions of Fe2 and Fe6. The stabilities of 57 representative structures are assessed by calculation of the reaction profiles and activation energies for the association and dissociation of N_2. Barriers to association of N_2 depend mainly on the location of the hydrogenation and the location of N_2 coordination, while dissociation barriers depend primarily on whether N_2 is η^2- and η^1-coordinated, and secondarily on the location of the hydrogenation. Increased negative charge on FeMo-co increases the barriers, while C in place of N at the center of FeMo-co has little effect. The interactions of the models of ligated FeMo-co with the surrounding protein, including proteins with mutations of key amino acids, are assessed by in silico cofactor transplantations and calculations of protein strain energies. From these results, which identify models involving contacts and interactions with the surrounding residues that have been shown by mutation to affect the N_2 activity of nitrogenase, and from the N_2 coordination profiles, it is concluded that endo-η^1-N_2 coordination at Fe6 is most probable. There is strong reason to believe that the mechanism of nitrogenase will involve one or more of the preferred models presented here, and a detailed foundation of structures and principles is now available for postulation and calculation of the profiles of the steps in which H atoms bound to FeMo-co are transferred to bound N_2.

Introduction

The enzyme nitrogenase effects the reduction of N_2 to NH_3 under mild conditions. While much is understood about the biochemical mechanism involving the two MoFe and Fe component proteins, and about the structure of the FeMo-cofactor (Figure 1a) where the reaction occurs, the intriguing chemical mechanism is still unknown.[1,2]

Key recent experiments involving proteins with modifications of residues in the vicinity of FeMoco have advanced knowledge of the mechanism.[3] In particular, the Fe2,Fe3,Fe6,Fe7 face of FeMoco, covered by α-70^{Val} (all residue labeling is from crystal structure 1M1N[4]), is identified as the locus of action, and more specifically the Fe2 and Fe6 atoms (Figure 1a) are implicated as the sites of binding of substrates and intermediates. The best spectroscopically characterized of the trapped species is from the reaction of the α-$70^{Val\rightarrow Ala}$ mutant MoFe protein with the alternative alkyne substrate propargyl alcohol (or propargyl amine) and is identified as the product allyl alcohol (or amine) η^2-bound to one Fe atom:[5] theoretical work has produced a detailed model for this alkyne substrate and alkene product bound to Fe6 of FeMoco within the surrounding protein.[6] There are strong reasons to believe that the catalyzed hydrogenations of N_2 and C_2H_2 occur in the same vicinity of FeMo-co.[7] Significant recent experiments have allowed the spectroscopic detection of nitrogenous species, believed to be N_2, MeNNH, and N_2H_4, trapped at 4 K in modified proteins.[8,9]

At this point, it is essential to know how N_2 can bind to the relevant atoms of FeMoco. FeMo-co has an unprecedented

(1) Burgess, B. K. *Chem. Rev.* **1990**, *90*, 1377−1406. Burris, R. H. *J. Biol. Chem.* **1991**, *266*, 9339−9342. Rees, D. C.; Chan, M. K.; Kim, J. *Adv. Inorg. Chem.* **1993**, *40*, 89−119. Peters, J. W.; Fisher, K.; Dean, D. R. *Annu. Rev. Microbiol.* **1995**, *49*, 335−366. Burgess, B. K.; Lowe, D. J. *Chem. Rev.* **1996**, *96*, 2983−3011. Seefeldt, L. C.; Dean, D. R. *Acc. Chem. Res.* **1997**, *30*, 260−266. Mayer, S. M.; Lawson, D. M.; Gormal, C. A.; Roe, S. M.; Smith, B. E. *J. Mol. Biol.* **1999**, *292*, 871−891. Rees, D. C.; Howard, J. B. *Curr. Opin. Chem. Biol.* **2000**, *4*, 559−566. Christiansen, J.; Dean, D. R.; Seefeldt, L. C. *Annu. Rev. Plant Physiol. Plant Mol. Biol.* **2001**, *52*, 269−295. Igarashi, R. Y.; Seefeldt, L. C. *Crit. Rev. Biochem. Mol. Biol.* **2003**, *38*, 351−384. Dos Santos, P. C.; Dean, D. R.; Hu, Y.; Ribbe, M. W. *Chem. Rev.* **2003**, *103*, 1159−1173. Seefeldt, L. C.; Dance, I. G.; Dean, D. R. *Biochemistry* **2004**, *43*, 1401−1409. Rees, D. C.; Tezcan, F. A.; Haynes, C. A.; Walton, M. Y.; Andrade, S.; Einsle, O.; Howard, J. A. *Philos. Trans. R. Soc. London, Ser. A* **2005**, *363*, 971−984. Peters, J. W.; Szilagyi, R. K. *Curr. Opin. Chem. Biol.* **2006**, *10*, 101−108.
(2) Smith, B. E. *Adv. Inorg. Chem.* **1999**, *47*, 159−218.
(3) Dos Santos, P. C.; Igarashi, R.; Lee, H.-I.; Hoffman, B. M.; Seefeldt, L. C.; Dean, D. R. *Acc. Chem. Res.* **2005**, *38*, 208−214.
(4) Einsle, O.; Tezcan, F. A.; Andrade, S. L. A.; Schmid, B.; Yoshida, M.; Howard, J. B.; Rees, D. C. *Science* **2002**, *297*, 1696−1700.
(5) Lee, H.-I.; Igarashi, R.; Laryukhin, M.; Doan, P. E.; Dos Santos, P. C.; Dean, D. R.; Seefeldt, L. C.; Hoffman, B. M. *J. Am. Chem. Soc.* **2004**, *126*, 9563−9569. Igarashi, R.; Dos Santos, P. C.; Niehaus, W. G.; Dance, I. G.; Dean, D. R.; Seefeldt, L. C. *J. Biol. Chem.* **2004**, *279*, 34770−34775.
(6) Dance, I. *J. Am. Chem. Soc.* **2004**, *126*, 11852−11863.
(7) Dance, I. *Biochemistry* **2006**, *45*, 6328−6340.

10.1021/ja0644428 CCC: $37.00

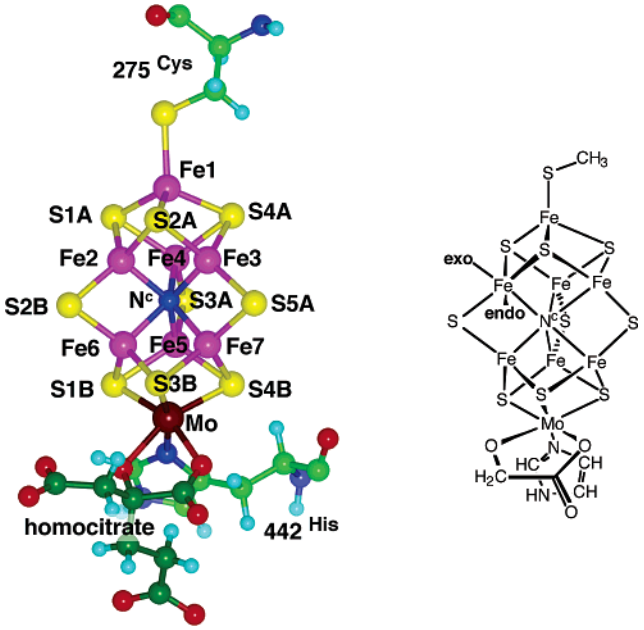

Figure 1. (a) The structure of FeMo-co, connected to the protein via α-275^{Cys} and α-442^{His} (*Azotobacter vinelandii*), with atom labeling for crystal structure 1M1N. The C atoms of homocitrate are dark green. (b) The exo and endo coordination positions at one Fe atom, marked on the model used in density functional calculations.

structure, not yet synthesized chemically, and the prospects for experimental access to the coordination chemistry of FeMo-co + N_2 under turnover conditions are not good. Reliable theoretical methods can provide insight into the otherwise inaccessible aspects of this coordination chemistry, which is the subject of this paper. There have been two prior theoretical investigations of N_2 binding to the full structure of FeMoco, one proposing Fe-η^1-N_2 coordination, stabilized by the presence of H atoms on the three μ-S atoms,[10] and the other proposing Fe−η^1-N_2 and Fe−N−N−Fe coordination with concomitant severance of an Fe−S bond.[11] These models are included in the full range of possible structures, which are assessed in this investigation, encompassing the exo and endo coordination sites at the central Fe atoms of FeMo-co (Figure 1b), and all bridging possibilities.

The binding of N_2 to FeMo-co is closely linked to the degree of reduction/hydrogenation of FeMo-co, and to the involvement of H_2, as illustrated in Figure 2, which is part of the mechanism developed by Thorneley and Lowe[12] to explain many kinetic data. The symbols E_n in the formulas of the intermediates give the number of preceding e^-/H^+(electronation/protonation) cycles. The key aspects of this scheme are that productive binding of N_2 occurs at the E_3H_3 and E_4H_4 reduced levels and involves reversible substitution of H_2, a process that could be associative or dissociative. This raises questions about how the binding of N_2 at the E_1H_1 and E_2H_2 levels might differ from that at E_3H_3,

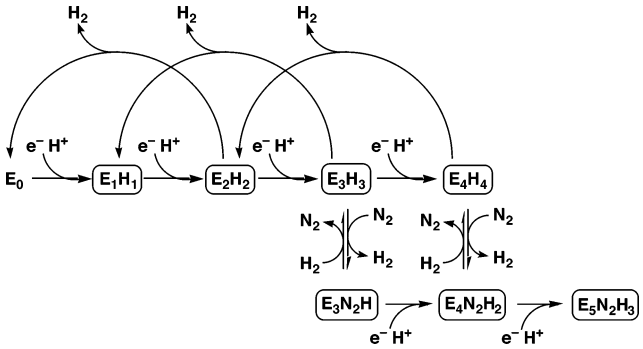

Figure 2. The early stages of the Thorneley−Lowe mechanism for the interactions of N_2 with various reduced states of FeMo-co.

E_4H_4 (the unproductivity via E_1H_1, E_2H_2 could be due to blocked subsequent steps), and how H atoms and H_2 molecules are bound with N_2 at FeMo-co. Accordingly, this investigation of the binding of N_2 involves FeMoco hydrogenated with 1, 2, 3, or 4 H atoms, and with bound H atoms plus an H_2 molecule, encompassing potential structures for all of the intermediates with initially bound N_2. I have detailed previously the preparatory hydrogenation of FeMoco, and my contention that all H atoms are introduced via S3B, from which they migrate to other Fe and S atoms and generate H_2.[7,13]

So, concurrent with the first experimental detection of bound N_2,[8] I report here a comprehensive investigation and evaluation of the coordination chemistry of FeMoco with N_2. The three main variables are (a) the coordination positions, exo and endo, at Fe2 and Fe6, (b) the η^1 (end) and η^2 (side) coordination modes for N_2, and (c) the degree of hydrogenation of FeMoco and the locations of bound H atoms and/or H_2 molecules. One question arising in the coordination chemistry of N_2 with FeMo-co is the effect of reduction by electronation alone as compared to reduction by hydrogenation (i.e., electronation plus concomitant protonation), and results relevant to this are presented, together with results bearing on the uncertainty about whether the atom at the center of FeMo-co is C rather than N. Investigations of the interactions between these models and the surrounding protein, including relevant mutants, are also reported.

The paper is organized to present first the structures and association/dissociation profiles for N_2 bound in the η^2 (type **1**) mode, the endo-η^1 (type **2**) mode, and the exo-η^1 (type **3**) mode, then the effects of increased negative charge on FeMo-co and the effects of C rather than N centering of FeMo-co, and finally the interactions of representative structures with surrounding protein.

Methodologies

The model used to calculate FeMo-co is Figure 1b, in which 442^{His} is truncated to imidazole, 275^{Cys} is truncated to SCH_3, and homocitrate is truncated to glycolate, $^-OCH_2COO^-$; this retains the native coordination of all metal atoms. The molecular oxidation state is defined by net charge of −3, as previously determined.[14]

(8) Barney, B. M.; Yang, T.-C.; Igarashi, R.; Dos Santos, P. C.; Laryukhin, M.; Lee, H.-I.; Hoffman, B. M.; Dean, D. R.; Seefeldt, L. C. *J. Am. Chem. Soc.* **2005**, *127*, 14960−14961. Barney, B. M.; Lee, H.-I.; Dos Santos, P. C.; Hoffman, B. M.; Dean, D. R.; Seefeldt, L. C. *Dalton Trans.* **2006**, 2277−2284.
(9) Barney, B. M.; Lukoyanov, D.; Yang, T.-C.; Dean, D. R.; Hoffman, B. M.; Seefeldt, L. C. *Proc. Natl. Acad. Sci. U.S.A.* **2006**, *103*, 17113−17118.
(10) Hinnemann, B.; Norskov, J. K. *J. Am. Chem. Soc.* **2004**, *126*, 3920−3927.
(11) Kastner, J.; Hemmen, S.; Blochl, P. E. *J. Chem. Phys.* **2005**, *123*, 074306.
(12) Lowe, D. J.; Thorneley, R. N. F. *Biochem. J.* **1984**, *224*, 877−886. Thorneley, R. N. F.; Lowe, D. J. Kinetics and Mechanism of the Nitrogenase Enzyme System. In *Molybdenum Enzymes*; Spiro, T. G., Ed.; Wiley-Interscience: New York, 1985; pp 221−284. Thorneley, R. N. F.; Lowe, D. J. *J. Biol. Inorg. Chem.* **1996**, *1*, 576−580.
(13) Dance, I. *J. Am. Chem. Soc.* **2005**, *127*, 10925−10942.
(14) Dance, I. *Inorg. Chem.* **2006**, *45*, 5084−5091.

Density functional calculations using the program DMol3 (version 3.2, 2005)[15] have been described previously.[7,13,14] A key feature of the calculations is the use of numerical basis sets including polarization functions (basis set dnp in DMol3). The functional is blyp, and the spin-unrestricted calculations are all-electron. Detailed validations of this DF methodology for FeMo-co and related systems, assessed against experimental data in terms of geometry and energy, have been published.[13] The errors associated with the DF calculations reported in this paper are estimated to be <0.05 Å in geometry, and <2 kcal mol^{-1} in energy.

The electronic structures of FeMo-co and its ligated forms have ca. 20 filled orbitals within 2 eV of the HOMO, and HOMO−LUMO gaps of ca. 0.4 eV. FeMo-co and its derivatives manifest alternative molecular spin states and electronic states that are usually close in energy (1−10 kcal mol^{-1}), and in geometry (although different electronic/spin states can have substantial differences in one Fe−N^c distance when it is long and nonbonding). These close-lying electronic states are characterized by variations in spin density, primarily at the metal atoms, and can be described and generated in terms of alternative distributions of individual metal spin states.[16] For the systems investigated in this paper, there are no relevant experimental data that could direct selection of the appropriate molecular electronic state (the enzyme is EPR silent during turnover), and therefore the lowest energy state was calculated (using the Fermi occupation option in DMol3). The lowest energy state almost always has the lowest molecular spin, $S = 0$ or $S = {}^1/_2$; a few of the optimized structures have $S = 1$ or $S = {}^3/_2$. For some of the ligated structures, it was evident (from erratic scf convergence) that alternative electronic/spin states were close, and for these species the electronic/spin state calculated was controlled by fixing orbital occupancy, or by specifying initial spin densities on metal atoms. As mentioned below, care was taken to follow one electronic state during calculation of reaction profiles.

Density functional calculations were performed on isolated complexes, without the protein surrounds. Representative structures were also optimized with a continuum solvation model to simulate the electronic effects of the protein surrounds. In this calculation, the charge distribution of ligated FeMo-co polarizes the dielectric medium and generates electrostatic energies. These calculations used the conductor-like screening model (COSMO) implemented in DMol,[17] with the van der Waals radii increased to S 2.1, Fe 2.5, Mo 2.8 Å. The results, using dielectric permittivities $\epsilon = 5$ and $\epsilon = 20$ for the surrounds, yielded negligible geometric differences (<0.05 Å) with the structures optimized in the gas-phase model. The magnitude of the effect on energy can be assessed from a system (**1-2H-e**, see Figure S1) where in the isolated molecule model the barrier for dissociation of η^2-N_2 is estimated to be 0.3 kcal mol^{-1}. A COSMO optimization with $\epsilon = 5$ retains bound N_2, while with $\epsilon = 20$ the N_2 just dissociates. Structure **1-1H(H$_2$)-a**, with a dissociation barrier of 0.7 kcal mol^{-1} in the absence of surrounds, also retains bound N_2 when calculated with a solvation dielectric of 20. From these results, it is concluded that the uncertainty in energy due to the use of the isolated molecule approximation is ca. 0.3 kcal mol^{-1} and less than 0.7 kcal mol^{-1} for the systems described in this paper.

For the calculation of transition states (TS) for the reactions of ligands on FeMo-co, conventional automated methods are foiled by the complexity of the vibrational and electronic structure of FeMo-co. It was found that the automated quadratic synchronous transit (QST) procedure[18] was sometimes compromised by changes in electronic state during the geometry excursions required to locate the saddle. The concomitant shifts in energy and gradient could then in QST generate erroneous transition states not connected on a single electronic state surface to the reactant and product structures. Further, for the case of ligand association/dissociation paths, an effectively dissociated geometry is arbitrarily defined. For these reasons, the following alternative procedure for location of the TS was developed, using manual interpolation of geometry and density functional evaluation of energy and energy gradient. The general procedure was to observe the initial changes in geometry and energy gradient during small-step energy minimizations from a geometry intermediate between reactant and product, and then to use this information to build a new intermediate geometry just on the other side of the barrier. Once geometries on either side of the barrier were obtained, careful iterative cycling between structures on *opposite* sides of the barrier, with diminishing geometry shifts and diminishing energy gradients, automatically optimizes all other variables while finding the lowest energy saddlepoint on the reaction coordinate. High accuracy can be achieved by continued iteration. The quality of each TS found was assessed via its low gradient, and by its energy minimization pathways to reactant and product when nudged. In this mapping of the reaction profile, the spin state and electronic states were monitored and controlled as necessary to ensure that a single electronic surface connected the reactant, transition, and product structures. This procedure is more reliable than the automated methods.

Optimizations of protein structure around ligated and unligated FeMo-co were made with the cvff force-field of the program Discover[3,19] supplemented with locally determined potentials for the coordination of 275^{Cys}, 442^{His}, and homocitrate to FeMo-co. The model was comprised of 1032 amino acids, 1332 associated water molecules, the P-cluster, and FeMo-co. The protein component was selected as all of chains A and B of the MoFe protein structure 1M1N, together with residues 494−523 of chain D, and all water molecules within 4 Å of these atoms or FeMo-co. This model is a thick protein sheath for FeMo-co and extends to the surface of the MoFe protein. All hydrogen atoms were included and energy-minimized to optimize the protein and the water hydrogen bonding. Nonbonded Coulombic energies were calculated with a dielectric constant numerically equal to the interatomic distance (Å). Intermolecular cutoff distances were 7 Å for van der Waals interactions and 9.5 Å for Coulombic interactions. Atoms of the P-cluster and of FeMo-co and its N_2/H/H_2 ligands were held fixed during energy minimization of all other components.

Results

A search for energy-minimized structures of FeMo-co coordinated by N_2, together with varying degrees of H/H_2 coordination at Fe and/or hydrogenation of S atoms, and restricting coordination to Fe2 and Fe6, revealed 94 different local energy wells. For a considerable number of postulated structures with η^2-N_2 coordination, no local energy well could be found, due to dissociation of N_2 or rearrangement to η^1-N_2 coordination. No energy minima were found for N_2 bridging two, three, or four Fe atoms of the Fe2, Fe3, Fe6, Fe7 face of FeMoco, with varying modes and degrees of hydrogenation of FeMo-co; instead, N_2 either dissociated or rearranged to η^1-N_2 coordination at a single Fe atom.

Assessment of the significance and stability of the many binding modes was made by calculation of the reaction profile for association and dissociation of N_2. For 57 representative

(15) Delley, B. *J. Chem. Phys.* **1990**, *92*, 508−517. Delley, B. DMol, a standard tool for density functional calculations: review and advances. In *Modern Density Functional Theory: a Tool for Chemistry*; Seminario, J. M., Politzer, P., Eds.; Elsevier: Amsterdam, 1995; Vol. 2, pp 221−254. Delley, B. *J. Chem. Phys.* **2000**, *113*, 7756−7764. *DMol3*; www.accelrys.com/mstudio/ms_modeling/dmol3.html, 2005.

(16) Lovell, T.; Li, J.; Liu, T.; Case, D. A.; Noodleman, L. *J. Am. Chem. Soc.* **2001**, *123*, 12392−12410. Lovell, T.; Li, J.; Case, D. A.; Noodleman, L. *J. Biol. Inorg. Chem.* **2002**, *7*, 735−749. Schimpl, J.; Petrilli, H. M.; Blochl, P. E. *J. Am. Chem. Soc.* **2003**, *125*, 15772−15778.

(17) Klamt, A.; Schüürmann, G. *J. Chem. Soc., Perkin Trans. 2* **1993**, 799−805. Andzelm, J.; Kolmel, C.; Klamt, A. *J. Chem. Phys.* **1995**, *103*, 9312−9320.

(18) Ayala, P. Y.; Schlegel, H. B. *J. Chem. Phys.* **1997**, *107*, 375−384.

(19) *Accelrys*; http://www.accelrys.com/products/datasheets/i2_discover_data.pdf, 2004.

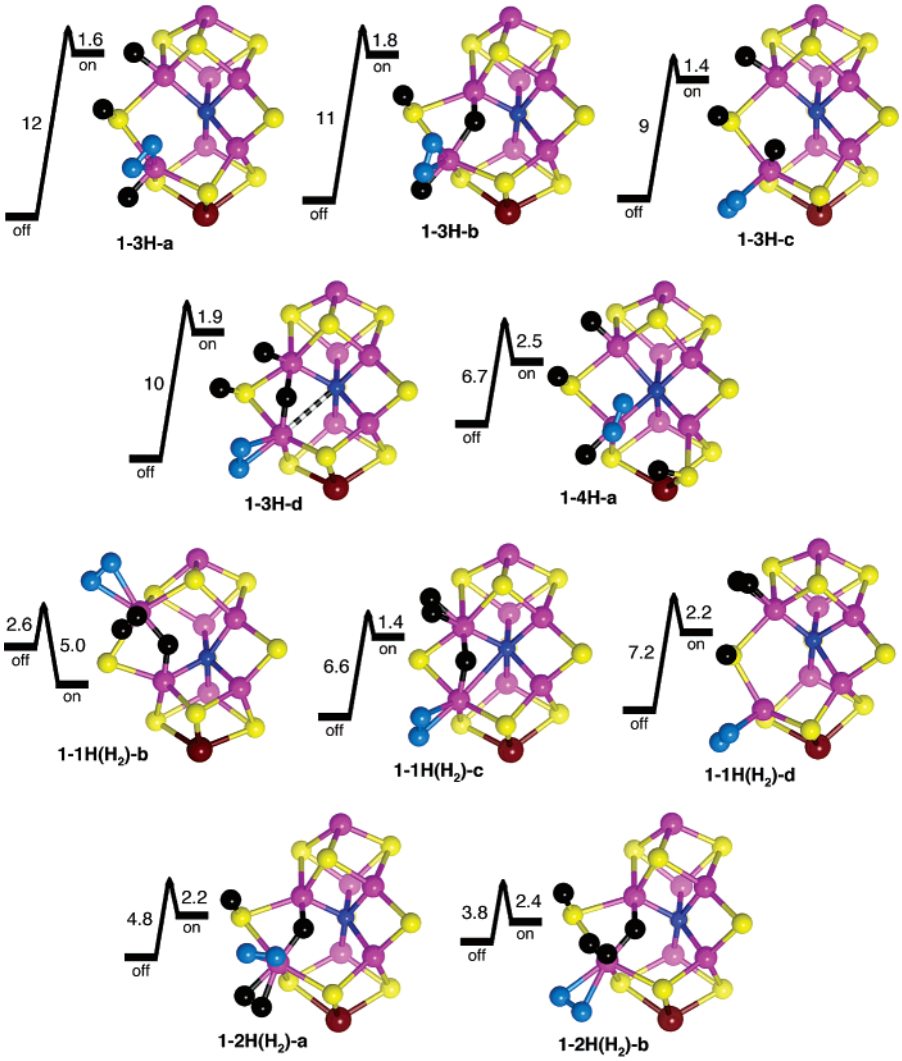

Figure 3. Some of the optimized models for η^2-N_2 coordinated at Fe6 or Fe2 of hydrogenated FeMo-co, together with the calculated activation energies (kcal mol^{-1}) for association and dissociation of N_2. The additional coordination of Fe1 (top) and Mo (bottom), included in the calculations, is not shown. The view direction is normal to the Fe2,Fe3,Fe6,Fe7 face. N_2 atoms are bright blue; bound H and H_2 atoms are black. The associated and dissociated states in the reaction profiles are labeled on and off, respectively. Supporting Information Figure S1 contains the complete set of results.

structures out of the 94, the transition state (TS) along the association/dissociation pathway was calculated. An uncoordinated (dissociated) structure was also obtained, by energy minimization beyond the TS until the relevant Fe−N distance was ca. 1 Å larger than that of the TS; this definition of the uncoordinated structure as Fe−N extended 1 Å beyond the transition structure is arbitrary, but in general was the point of reduced gradient for further separation, and is suitable for comparison of structures. The activation energies for association and dissociation were calculated from the energies of the bound state, of the TS, and of the dissociated state; these activation energies are plotted on the figures presenting the structures. These are results for isolated molecules: the errors due to neglect of the electronic influences of the protein surrounds are estimated to be <0.05 Å in geometry and <0.5 kcal mol^{-1} in energy. The steric influences of the surrounding protein are discussed later.

In general, the optimized structures have the lowest possible molecular spin, $S = 0$ or $S = {}^1/_2$. The calculated partial charges on the bound N and H atoms range from −0.25e to +0.25e, and the calculated spins are <0.09 on H and <0.01 on N.

The results are presented in three coordination groups, first those with η^2-coordinated N_2 (type **1**), then those with η^1-N_2 in the endo coordination position of Fe (type **2**), and finally those with η^1-N_2 in the exo coordination position of Fe (type **3**). The structure labeling notation to be used gives first the type number, then the number of H atoms, then H_2 if present, and finally a lower case differentiating letter, for example, **1-2H(H_2)-a**. The results are presented pictorially; all of the structural figures are oriented in the same way, looking directly at the Fe2,Fe3,Fe6,-Fe7 face, with Fe1 at the top and Mo at the bottom. All structure pictures omit the additional coordination of Fe1 and Mo, included in the calculations. The profiles plot the relative energies of the state with N_2 unbound (labeled "off"), then the transition state, and then the state with N_2 coordinated (labeled "on"). The activation barriers (kcal mol^{-1}) for the association (left side) and dissociation (right side) of N_2 are given on each profile. All of the profiles are plotted on the same energy scale, to emphasize the variations. The calculations have concentrated on the binding of N_2 at Fe6, which is believed to be most probable,[7] but some results for N_2 binding at Fe2 are provided; in general, the differences between Fe2 and Fe6 are minor.

η^2-Coordinated N_2 (Type 1). Figure 3 presents structures and association/dissociation profiles for 10 representative structures with η^2-coordinated N_2, all at the E_3 or E_4 reduction levels. The full set of 43 different structures and 25 profiles, for all reduction levels, is contained in Figure S1 (Supporting Information). The presentation is arranged in order of increasing number of H atoms, followed by structures containing also bound H_2. Note the geometrical diversity in Figure 3.

The complete results reveal the structural principles for η^2-coordination of N_2 to FeMo-co: (1) η^2-N_2 can be bound in a distinctly endo coordination position when an H atom (e.g., **1-3H-a**) or H_2 molecule (e.g., **1-2H(H_2)-a**) is exo on the same Fe atom, or otherwise the N_2 can be in the exo coordination position; (2) hydrogenation of S3B, in one of several conformations,[13] generally elongates Fe6−S3B, which in turn affects the stereochemistry of N_2-coordinated Fe6, and allows N_2 to be coordinated in a position intermediate between endo and exo when there is no other ligation of the Fe atom (Fig S1); (3) one Fe−N^c interaction can be elongated to over 3 Å, but two or more cannot, which is another manifestation of the coordinative allosteric control exerted by N^c;[13] (4) regarding N_2 as one ligand, Fe6 can be four-, five-, or six-coordinate; (5) H bridging Fe2 and Fe6 can occur with retention of both Fe−N^c bonds (e.g., **1-1H(H_2)-c**), or it can take the place of one Fe−N^c bond (e.g., **1-3H-b**, **1-2H(H_2)-b**); (6) when η^2-N_2 and η^2-H_2 are bound to the same Fe atom their molecular axes are approximately parallel, but other twistomers for η^2-N_2−Fe are possible when H_2 is not present (for example, contrast **1-3H-b** and **1-2H(H_2)-a** in Figure 3); and (7) the structures with η^2-N_2 plus H and/or H_2 bound to FeMo-co are generally similar to the structures with η^2-H_2 plus H bound to FeMo-co.[13]

Turning to the profiles for association and dissociation of η^2-N_2, the prominent result is that the barrier for dissociation of N_2 is generally about 2 kcal mol^{-1} for this set of diverse structures (mean = 2.5 kcal mol^{-1} for 25 profiles) and is not greater than 5 kcal mol^{-1}. For η^2-N_2 bound exo to Fe6, with no hydrogenation (Figure S1), the barrier for dissociation is 5.3 kcal mol^{-1}, and it appears that this is an upper limit to the activation energy for dissociation of η^2-N_2. In all cases except one (**1-1H(H_2)-b**), the barrier to association of η^2-N_2 is larger than the barrier for dissociation. The associative approach to the transition state involves varying degrees of preparatory change in the FeMo-co structure, such as changes in the Fe−N^c distance, or an opening of the S2B−Fe6−S3B angle preparatory to N_2 binding in an endo position, and to some extent the magnitude of the barrier to association can be correlated with the nature and completeness of the coordination of Fe prior to binding, and with the size of the changes required to reach the transition geometry. Thus, the largest barrier to association, in **1-1H-e**, involves extension of Fe6−N^c from 2.1 to 2.7 Å and concomitant reduction from four to three coordination of Fe6. The smallest association barriers occur in structures such as **1-1H-b**, **1-1H(H_2)-b**, **1-2H(H_2)-b**, where Fe has good square pyramidal five-coordination prior to N_2 binding. Fe−N(N_2) distances in the transition states range from 2.45 to 2.7 Å, while the Fe−N(N_2) distances for the bound structures are generally 2.2 Å.

A considerable number (ca. 30) of postulated structures with η^2-N_2 did not yield a local energy minimum with bound N_2. In particular, endo-η^2-N_2 is often unstable; the stable structures presented in Figures 3 and S1 are the only ones found. A number of results indicate that the presence of an H atom on S2B stabilizes the binding of η^2-N_2. Thus, stable structures **1-2H-d**, **1-3H-a**, and **1-3H-b**, all with S2B-H, instead dissociate N_2 without barrier if the H atom on S2B is absent. Further, the increase in dissociation barrier from 0.7 kcal mol^{-1} in **1-1H-(H_2)-a** to 2.2 kcal mol^{-1} in **1-2H(H_2)-a** can be attributed to S2B-H.

Finally, in some instances, it was observed that the η^2-N_2 coordination is unsymmetrical, and occasionally there is a very small or nonexistent barrier between η^2-coordination and more stable η^1-coordination of N_2: that is, side-bound N_2 can unhook to become end-bound.

Endo η^1-Coordinated N_2 (Type 2). Some structures and profiles for η^1-coordination of N_2 at the endo position of Fe are illustrated in Figure 4, with the full results in Figure S2. The geometrical distortions of FeMo-co and the locations of H atoms and H_2 molecules are similar to those already described. Isomers that have the same distribution of H/H_2 and differ only in the endo-η^2-N_2 or endo-η^1-N_2 coordination have essentially the same geometries. However, the association/dissociation energy profiles are distinctly different. In particular, the barrier for dissociation of N_2 has increased and ranges 7−21 kcal mol^{-1} with an average of 13.3 kcal mol^{-1} (for 20 profiles). Barriers for association range from 3 to 20 kcal mol^{-1} and average 8.3 kcal mol^{-1}. Clearly, η^1-N_2 is more tightly bound than η^2-N_2, and the majority of the structures now have net exergonic binding of N_2. In the transition states, the Fe−N distance is generally in the range 2.6−2.7 Å, with extremes of 2.4 and 2.9 Å; the bound Fe−N distance ranges 1.80−1.84 Å.

Several patterns are evident. (1) The presence of a hydrogen atom on S2B increases the barrier for dissociation of N_2: compare **2-1H-a** and **2-2H-c** (increase of 7 kcal mol^{-1}), **2-2H-a** and **2-3H-a** (increase of 9 kcal mol^{-1}), and **2-2H-b** and **2-3H-b** (increase of 5 kcal mol^{-1}). (2) Structures with an Fe2−H−Fe6 bridge and with η^1-N_2−Fe detached from N^c (i.e., **2-2H-b**, **2-3H-b**, **2-1H(H_2)-c**, **2-1H(H_2)-f**) have the largest barriers for dissociation. (3) Smaller activation energies for association of N_2 occur where the prior coordination of Fe is good five-coordination, and particularly where H_2 is part of the prior coordination (e.g., **2-1H(H_2)-c**, **2-1H(H_2)-f**, **2-2H(H_2)-a**).

In general, there is similar behavior at Fe2 and Fe6, but differing reaction profiles for one pair of related structures that are Fe6/Fe2 invertomers, interchanging the coordination at Fe2 and Fe6, are significant. **2-1H(H_2)-a** has endo-η^1-N_2 and exo-H at Fe6 with exo-H at Fe2, while **2-1H(H_2)-b** has the inverse, endo-η^1-N_2 and exo-H at Fe2 with exo-H at Fe6 (Figure 5). With N_2 at Fe6, **2-1H(H_2)-a** shows normal profiles for association and dissociation of N_2. Yet the invertomer behaves differently, and, as illustrated in Figure 5, when the association of N_2 is almost complete at Fe2 (**2-1H(H_2)-b**), a barrierless dissociation of the H_2 on Fe6 commences. That is, H_2 is stable on Fe6 until but not after the coordination of N_2 at Fe2. These results are another manifestation of "end-differentiation" in the FeMo-co core[13] and of coordinative allosterism[13] in which events at one Fe affect events at another Fe atom, via N^c. The behavior of **2-1H(H_2)-b** in which coordination of N_2 at one Fe causes dissociation of H_2 at another is relevant to the under-

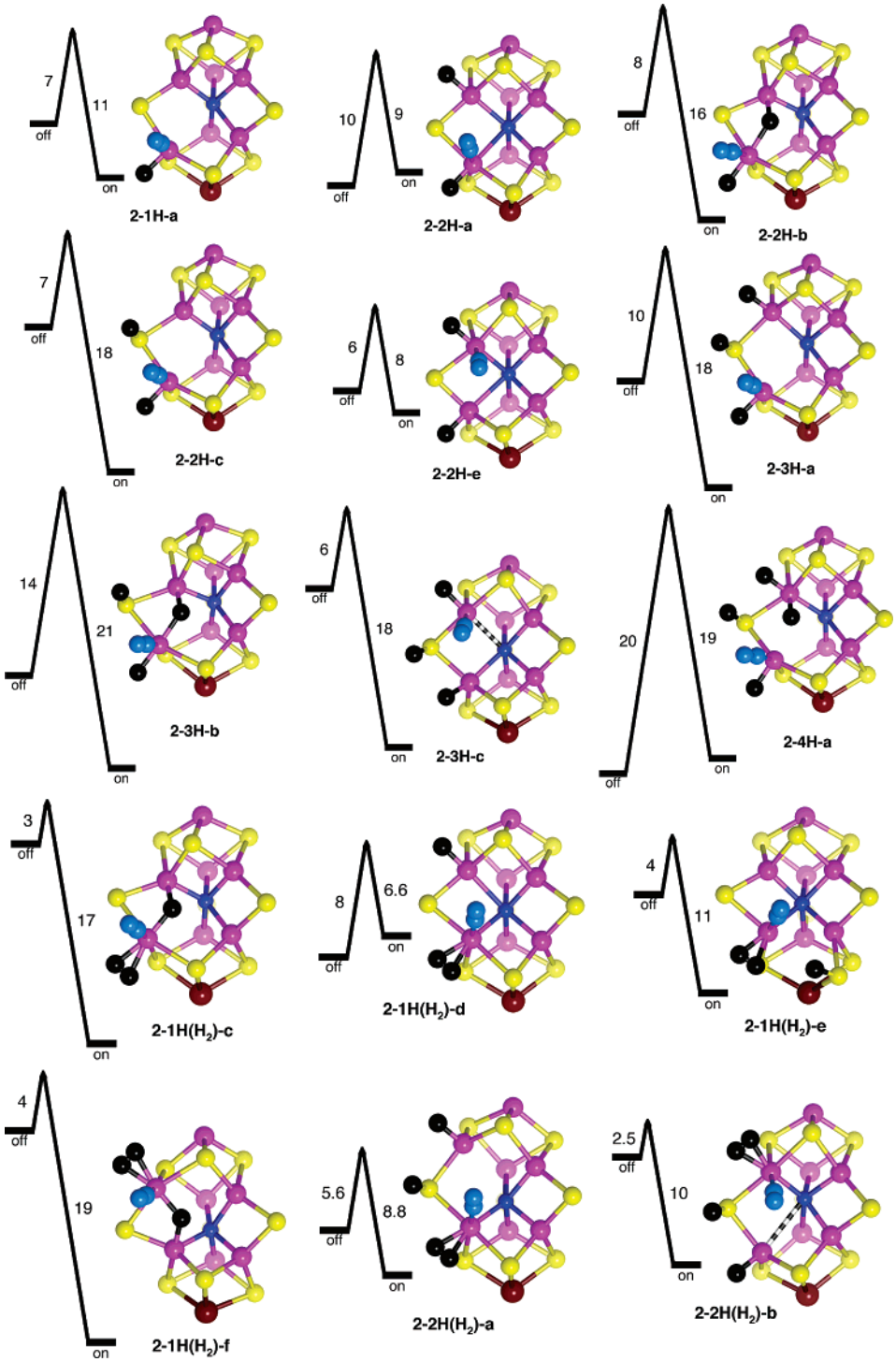

Figure 4. Some of the optimized models for η^1-N_2 coordinated at the endo position of Fe6 or Fe2 of hydrogenated FeMo-co, together with the calculated activation energies (kcal mol^{-1}) for association and dissociation of N_2. The N_2 molecule is directed approximately perpendicular to the Fe_4 face, which is toward the viewer. Supporting Information Figure S2 contains the complete set of results.

standing of the experimental data which link, temporally and stoichiometrically, the binding of N_2 with the evolution of H_2 (Figure 2).

Exo η^1-Coordinated N_2 (Type 3). The calculated structures and profiles are illustrated in Figure 6 and provided in full in Figure S3. In general, the structural features are similar to those already described. A noticeable feature is the prevalence of structures with (i) an Fe2−H−Fe6 bridge, (ii) both Fe−N^c ca. 2.2 Å, and (iii) exo-ligation of both Fe2 and Fe6. Comparison of related structures with exo-η^1-N_2 or exo-η^2-N_2 coordination (Figures 3, S1) shows that Fe−N^c with exo-η^1-N_2 coordination is usually shorter; that is, trans η^1-N_2−Fe−N^c coordination is geometrically tighter than trans η^2-N_2−Fe−N^c coordination. In the transition states, the Fe−N distance generally ranges 2.6−2.7 Å, with bound Fe−N distances ca. 1.83 Å. Structure **3-1H-(H_2)-b** with a detached Fe6−H−Fe2 bridge is remarkable in that the Fe6−N distance in the transition state is unusually long, 2.9 Å, almost 1.1 Å longer than the bond in the associated structure. A similar structure with endo-η^1-N_2, **2-1H(H_2)-c**, also has an unusually elongated (Fe−N 2.9 Å) transition state.

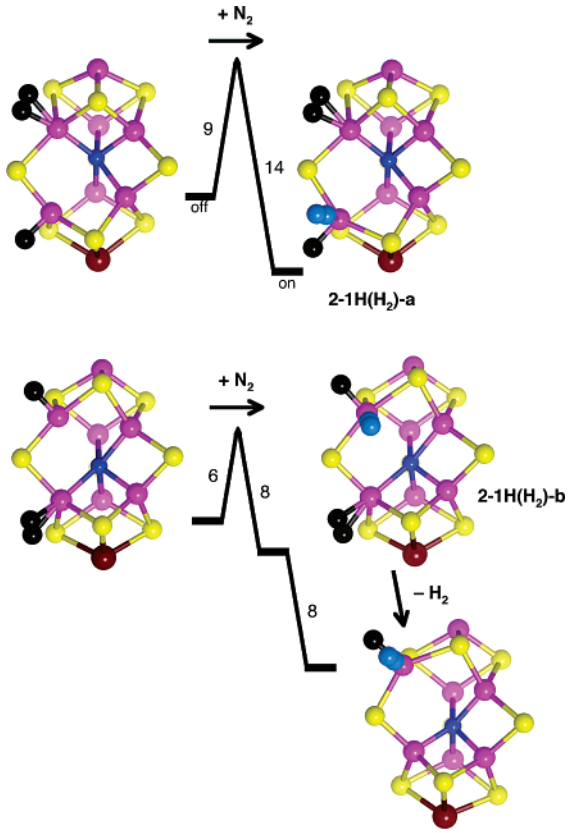

Figure 5. The differing behaviors of the **2-1H(H_2)-a** and **2-1H(H_2)-b** systems: energies in kcal mol^{-1}. A normal association/dissociation equilibrium occurs for **2-1H(H_2)-a**, but, when there is interchanged ligation at Fe2 and Fe6, **2-1H(H_2)-b** undergoes barrierless dissociation of H_2 after coordination of N_2.

Generally the association barriers for exo-η^1-N_2 coordination are slightly smaller (mean 5.9 kcal mol^{-1}, 12 values) than those for endo-η^1-N_2 coordination (mean 8.3 kcal mol^{-1}). At least part of this can be attributed to the fact that S2B does not need to be folded back to prepare for exo coordination, as it does for endo coordination at Fe2 or Fe6. The mean activation energy for dissociation of exo-η^1-N_2 is 15.3 kcal mol^{-1}, slightly larger than that for endo η^1-N_2.

Overall, the primary result for coordination of N_2 is that η^2-N_2-coordination is weak and endergonic while η^1-N_2-coordination is comparatively strong and exergonic, with a slightly smaller association barrier and larger dissociation barrier for η^1-N_2-coordination in the exo position relative to the endo position. There is an equally significant secondary result, which is that the distribution of H atoms and possibly an H_2 molecule can have a larger and dominant influence on the coordination geometries and dynamics. In this context, a fundamental question is whether increased hydrogenation of FeMo-co facilitates its binding of N_2, as is suggested by the Thorneley–Lowe kinetic scheme (Figure 2). Some responses to this question can be drawn from the results for η^1-N_2-coordination. The complete set of profiles for endo-η^1-N_2-coordination (Figure S2) does not show a statistically significant trend in dissociation barriers with degree of hydrogenation, but the dissociation barriers for exo-η^1-N_2-coordination (Figure S3) increase with hydrogenation: mean barriers (and number of profiles) are 6.8 (1) for E_0, 12.8 (3) for E_1H_1, 14 (3) for E_2H_2, 19 (4) for E_3H_3, and 21 (1) kcal mol^{-1} for E_4H_4. However, again the location of the hydrogenation is important. Two pairs of structures, **3-1H-(H_2)-a**/**3-2H-a** (Figure 6), and **3-2H(H_2)-a**/**3-3H-a** (Figure 6), show clearly that H_2 rather than H on the other Fe, not bearing N_2, increases the barriers for both association and dissociation of N_2. In the pair **2-1H(H_2)-a**/**2-2H-a** with endo rather than exo-N_2, the presence of H_2 rather than H on the other Fe increases only the barrier for dissociation of N_2. If, instead, the comparison involves H_2 versus H on the same Fe that bears N_2, the effect of H_2 is the opposite, decreasing barriers: the instances of this are **2-2H(H_2)-b**/**2-3H-c** (Figure 4), **2-1H(H_2)-c**/**2-2H-b** (Figure 4), and **2-1H(H_2)-d**/**2-2H-a** (Figure 4).

Binding of N_2 to More Negatively Charged FeMo-co. In the preceding it has been assumed that the electronation and protonation steps occur together, and therefore that the hydrogenated FeMo-co that binds N_2 has the same charge state as resting FeMo-co. Alternatively stated, the assumption has been that the binding of N_2 to FeMo-co does not occur immediately after electron transfer to FeMo-co and before subsequent protonation. This is consistent with all interpretations of the kinetic data. Nevertheless, there is a question about the coordination chemistry: how is the association and dissociation of N_2 affected by additional negative charge on FeMo-co? This has been investigated, by calculating the association/dissociation profiles for a number of species with a charge of −4 rather than −3. Table 1 presents the activation energies, in comparison with those reported above for charge −3. In all cases, the activation energies for charge −4 are greater than those for charge −3.

What If the Central Atom of FeMo-co Is C Rather than N? Despite careful spectroscopic investigation,[20] there is still no direct experimental evidence for the identity of the atom at the center of FeMo-co, labeled N^c in Figure 1. A number of theoretical investigations point to N and C as the possibilities.[21] Using a method that correlates experimental redox potentials for FeMo-co and comparable reference compounds,[14] and on the basis of the nonbiological chemistry that would be expected in the biosynthesis of C-centered FeMo-co, I have previously concluded[14] that the central atom is more likely to be N. Nevertheless, the issue is not resolved experimentally, and the obvious question here is how the coordination chemistry of N_2 with C-centered FeMo-co would differ from that described above for N-centered FeMo-co. Optimized structures for bound N_2 and reaction profiles have been determined for four C-centered homologues (with model charge −4 to maintain the correct electron count), and the comparisons are made in Table 2. There is little difference between the structures and the coordination profiles for C- and N-centered FeMo-co. The largest discrepancy occurs in **2-2H(H_2)-a**, where the Fe2−C^c distance is 2.4 Å while the Fe2−N^c distance is 3.0 Å, and the activation energy for dissociation of N_2 is 13 kcal mol^{-1} for X = C as compared to 8.8 kcal mol^{-1} for X = N.

Interactions with Surrounding Protein. So far the influence of the surrounding protein on the coordination of N_2 to FeMo-co has been incorporated only to the extent that site-directed mutagenic data focus attention on Fe6 and Fe2 as the coordina-

(20) Lee, H.-I.; Benton, P. M. C.; Laryukhin, M.; Igarashi, R. Y.; Dean, D. R.; Seefeldt, L. C.; Hoffman, B. M. *J. Am. Chem. Soc.* **2003**, *125*, 5604−5605. Yang, T.-C.; Maeser, N. K.; Laryukhin, M.; Lee, H.-I.; Dean, D. R.; Seefeldt, L. C.; Hoffman, B. M. *J. Am. Chem. Soc.* **2005**, *127*, 12804−12805.

(21) Dance, I. *Chem. Commun.* **2003**, 324−325. Lovell, T.; Liu, T.; Case, D. A.; Noodleman, L. *J. Am. Chem. Soc.* **2003**, *125*, 8377−8383. Vrajmasu, V.; Munck, E.; Bominaar, E. L. *Inorg. Chem.* **2003**, *42*, 5974−5988.

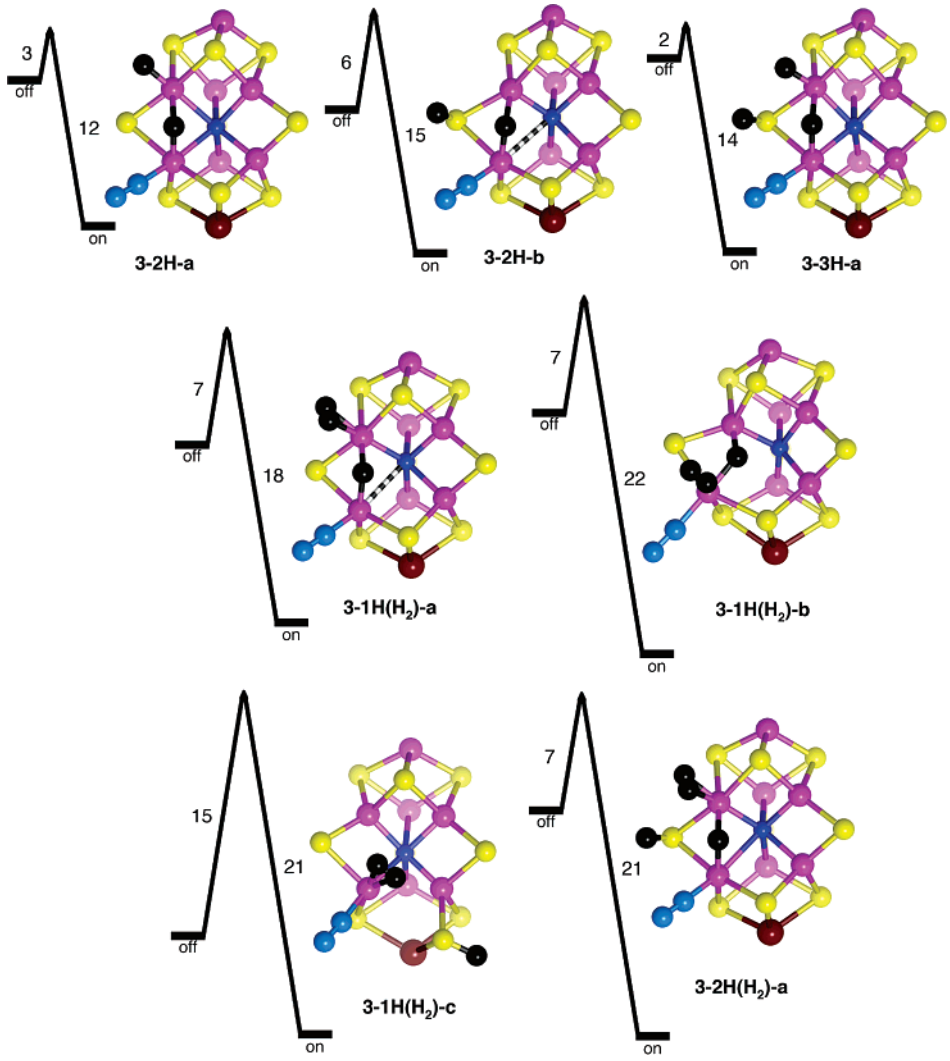

Figure 6. Some of the optimized models for η^1-N_2 coordinated at the exo position of Fe6 or Fe2 of hydrogenated FeMo-co, together with the calculated activation energies (kcal mol^{-1}) for association and dissociation of N_2. Supporting Information Figure S3 contains the complete set of results.

Table 1. Activation Energies (kcal mol^{-1}) for Association and Dissociation of N_2 with Electronated FeMo-co Species (Charge −4) in Comparison with Results for Charge −3

	charge −4		charge −3	
structure	association	dissociation	association	dissociation
1-1H-c	11	7.8	6.3	2.6
1-2H-d	11.5	2.0	6.9	1.9
2-1H-a	13	9	11	7
2-1H(H_2)-d	9	8.4	8	6.6
3-a	6	12	3.8	6.8
3-2H-a	4	12	3	12
3-2H-b	7	23	6	15

Table 2. Comparisons of the Activation Energies (kcal mol^{-1}) for Association/Dissociation of N_2 for C-Centered Homologues of N-Centered FeMo-co Structures

	X = C		X = N	
structure	association	dissociation	association	dissociation
1-3H-a	14	2.6	12	1.6
2-2H-a	9	12	10	9
2-2H(H_2)-a	7	13	5.6	8.8
3-3H-a	3	11	2	14

tion sites. I now examine specific interactions between N_2-ligated FeMo-co and the protein in which it is embedded. The initial questions are: (a) whether the various models for N_2 plus H/H_2 coordination of FeMo-co will fit into the protein? (b) What movements of surrounding protein might be required for N_2 binding, and what energy penalties might these incur? (c) Which models are consistent with the biochemical data on N_2 binding to proteins with mutated surrounding residues?

The relevant experimental data about influential surrounding residues are: (i) an increase in the size of the side-chain of residue α-70, from valine [$CH(CH_3)_2$] to isoleucine [$CH(CH_3)(CH_2CH_3)$], severely diminishes the reduction of N_2 (and of all other susbstrates except H^+);[22] (ii) mutation of residue α-69 from glycine to serine does not change the wild-type behavior of N_2, but does change the behavior of C_2H_2;[23] (iii) modification of α-195 from histidine to glutamine or asparagine does not affect the binding of N_2 but does interfere with the hydrogenation of N_2;[24,25] (iv) the α-191$^{Gln\rightarrow Lys}$ mutant does not

(22) Barney, B. M.; Igarashi, R. Y.; Dos Santos, P. C.; Dean, D. R.; Seefeldt, L. C. *J. Biol. Chem.* **2004**, *279*, 53621−53624.
(23) Christiansen, J.; Cash, V. L.; Seefeldt, L. C.; Dean, D. R. *J. Biol. Chem.* **2000**, *275*, 11459−11464. Christiansen, J.; Seefeldt, L. C.; Dean, D. R. *J. Biol. Chem.* **2000**, *275*, 36104−36107.
(24) Kim, C. H.; Newton, W. E.; Dean, D. R. *Biochemistry* **1995**, *34*, 2798−2808. Dilworth, M. J.; Fisher, K.; Kim, C. H.; Newton, W. E. *Biochemistry* **1998**, *37*, 17495−17505.
(25) Fisher, K.; Dilworth, M. J.; Newton, W. E. *Biochemistry* **2000**, *39*, 15570−15577.

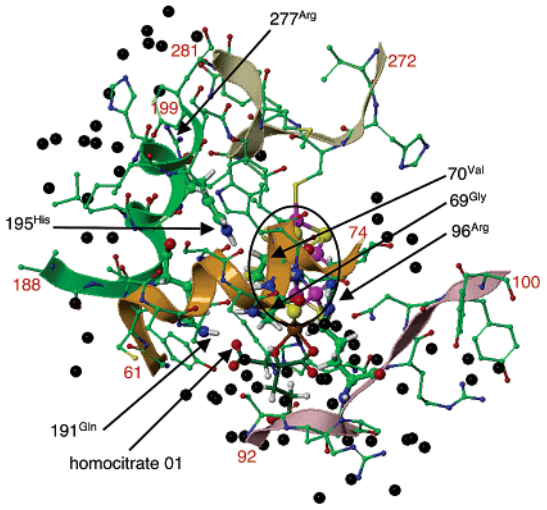

Figure 7. The significant components of the MoFe protein (optimized, see Methodologies) surrounding the active face (enclosed with black oval) of FeMo-co, viewed in the standard orientation normal to the face. The side-chains of influential residues are arrowed, as is the uncoordinated carboxylate of homocitrate containing atom O1. Residue numbers at the ends of the four relevant polypeptide sequences (61−74, orange; 92−100, pink; 188−199, green; 272−281, gray) are labeled in red: all residues are in the α-chain of structure 1M1N. Water O atoms within 7 Å of FeMoco or within 3 Å of residues shown are marked black.

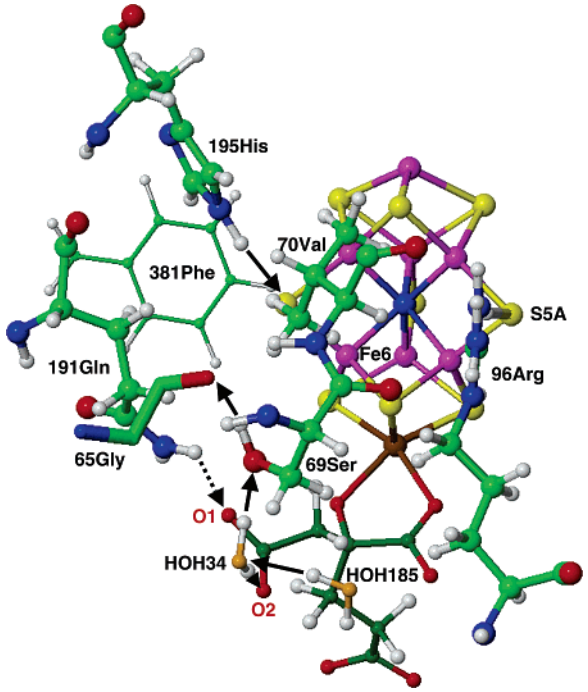

Figure 8. Key features of the immediate surrounds of FeMo-co relevant to the coordination of N_2, viewed close to the standard direction. Homocitrate C atoms are dark green, and water oxygen atoms are orange: α-65^{Gly} is partially drawn, with thick bonds, and α-381^{Phe} is drawn only as the side-chain with thin bonds. The hydrogen bonds from α-195^{His} to S2B and from α-96^{Arg} to S5A are evident. The α-69$^{Gly\rightarrow Ser}$ mutant is shown, in the side-chain conformation that forms a hydrogen bond to α-65:CO and from water34, which also has hydrogen bonds from water185 and to homocitrate O2. This weakens the hydrogen bond from the amide side-chain of α-191^{Gln} to O1 of homocitrate, marked as a dotted arrow. This hydrogen bond is normal in the other two conformations of α-69^{Ser} and in wild-type α-69^{Gly}.

interact with N_2;[25] (v) modification of α-277^{Arg} diminishes and changes the general reactivity of ntrogenase, with the α-277^{His} mutant being totally unresponsive to N_2 although not with the larger substrate C_2H_2;[26] (vi) α-96$^{Arg\rightarrow Gln}$ mutation slows diazotropic growth;[27] and (vii) the α-381$^{Phe\rightarrow Arg}$ strain does not grow on N_2.[2,27]

Figure 7 shows the components of the MoFe protein that are relevant to considerations of the mutual interactions between ligated FeMo-co and its surroundings (residues at the back, away from the front Fe2,Fe3,Fe6,Fe7 face, block ligation but stabilize the connection between FeMo-co and protein). There are four polypeptide segments, all in the α-chain. At the Mo (southern) end of FeMo-co, the unstructured segment α-92−100 (pink) passes through the aqueous domain surrounding homocitrate: the side-chain of α-96^{Arg} extends from this domain to hydrogen bond to S5A, which bridges Fe3 and Fe7 of FeMo-co. At the Fe1 (northern) end, the unstructured segment from α-272 to α-281 contains α-275^{Cys}, which anchors Fe1, and α-277^{Arg} whose arginine group is 9 Å from FeMo-co. The other two domains have α-helical structure. The front face helix (Figure 7, orange, residues α-61 to α-74) contains the crucial residues α-70^{Val} and α-69^{Gly}. From the green helix (residues α-189 to α-199), the side-chains of α-195^{His} and α-191^{Gln} extend toward FeMo-co. Figure 7 emphasizes the positions of all of the water molecules in these domains and shows that the orange and green helices are in contact and that the region of their interface is hydrophobic and free of water molecules. Ligation of FeMo-co at Fe6 and/or Fe2 impinges directly on the side-chains of residues in the orange and green helices.

To evaluate the interactions between ligated FeMo-co and its surrounds, I use a general procedure involving in silico cofactor transplantation, in which the atoms of the transplant cofactor are superimposed (by least-square displacements of Fe, Mo, and S atoms) on the existing cofactor, which is then deleted. In the first stage of this analysis, the cofactor ligated with N_2 and H/H_2 is substituted for unligated FeMo-co in the MoFe protein (represented by a force-field-optimized section of PDB 1M1N, containing 1332 residues and 1032 water molecules with all hydrogen atoms). Contacts between the $N_2/H/H_2$ ligands and surrounding polypeptide are checked, α-70^{Val} is moved away if necessary, and then the structure is relaxed by (force-field) energy minimization of the polypeptide plus water components while the ligated FeMo-co is held rigid. This yields an optimized structure for the protein containing embedded ligated FeMo-co, the protein structure of which is examined for modifications of residue positions, water positions, and important hydrogen bonds. Next, in a second stage to assess the energies associated with these modifications, unligated FeMo-co is transplanted back into the modified-protein structure, and the composite is relaxed back to the original resting structure. The energy change during the protein relaxation with unligated FeMo-co is a measure of the protein strain energy required to accommodate the ligated FeMo-co. This overall procedure provides relative measures of the geometric and energetic consequences, in proteo, of the various models for N_2 bound to hydrogenated FeMo-co. Two points need to be recognized in this analysis. First, the calculated protein strain energy is not that associated with a mechanistic step involving coordination of N_2, for which the pre-hydrogenated FeMo-co rather than bare FeMo-co would be the reference state and energy. Second, uncertainties in the calculated energies arise from the possibility of alternative relaxation pathways (i.e.,

(26) Shen, J.; Dean, D. R.; Newton, W. E. *Biochemistry* **1997**, *36*, 4884−4894.
(27) Newton, W. E.; Dean, D. R. *ACS Symp. Ser.* **1993**, *535*, 216−230.

Table 3. Structures and Protein Strain Energies for N_2-Ligated FeMo-co Models within the MoFe Protein and Some Mutant Proteins

N_2 coordination	model[a]	protein	increase in N^c–70:Cα distance Å	strain energy kcal mol^{-1}	hydrogen bonding[b] Å, deg
exo-Fe6-η^2	**1-3H-c**	WT	0	22	S2BH→195:Nϵ, 2.66, 133 191:NHϵ→N_2, 2.07, 158
	1-3H-c	69^{Ser}	0	12	S2BH→195:Nϵ, 2.63, 135 191:NHϵ→N_2, 2.11, 152
	1-2H(H_2)-b	WT	0.2	50	S2BH→195:Nϵ, 2.40, 163 191:NHϵ→N_2, 1.99, 146
	1-2H(H_2)-b	69^{Ser}	0.4	40	S2BH→195:Nϵ, 2.43, 161 191:NHϵ→N_2, 2.28, 129
endo-Fe6-η^2	**1-3H-a**	WT	0	33	S2BH→195:Nϵ, 2.74, 139 191:NHϵ→HCA, 2.37, 142
	1-3H-a	70^{Ile}	0.7	57	S2BH→195:Nϵ, 2.60, 142 191:NHϵ→HCA, 2.27, 126
	1-3H-a	69^{Ser}	0.2	33	S2BH→195:Nϵ, 2.76, 143
	1-3H-a: TS	69^{Ser}	0.2	45	S2BH→195:Nϵ, 2.83, 141
exo-Fe6-η^1	**3-3H-a**	WT	0	29	S2BH→195:Nϵ, 3.03, 135 191:NHϵ→HCA, 2.29, 127 191:NHϵ→N_2, 2.37, 149
	3-3H-a	381^{Arg}	0	28	S2BH→195:Nϵ, 3.01, 137 191:NHϵ→N_2, 2.32, 150
	3-3H-a	70^{Ile}	0.2	35	S2BH→195:Nϵ, 3.05, 137 191:NHϵ→HCA, 2.21, 124 191:NHϵ→N_2, 2.27, 150
	3-3H-a	69^{Ser}	0.2	18	S2BH→195:Nϵ, 3.03, 139 191:NHϵ→N_2, 2.28, 151
	3-3H-a: TS	69^{Ser}	0	32	S2BH→195:Nϵ, 2.94, 138 191:NHϵ→N_2, 2.32, 149
endo-Fe6-η^1	**2-1H(H_2)-e**	69^{Ser}	0	42	195:Hϵ→S2B, 2.58, 134
	2-2H(H_2)-a	WT	0.5	42	S2BH→195:Nϵ, 2.56, 141 191:NHϵ→HCA, 2.21, 150
	2-2H(H_2)-a: TS	WT	0.7	75	S2BH→195:Nϵ, 2.86, 124 191:NHϵ→HCA, 1.79, 159
	2-2H(H_2)-a	69^{Ser}	0.4	40	S2BHf195:Nϵ, 2.74, 138 191:NHϵ→HCA, 2.73, 143
	2-2H(H_2)-a: TS	69^{Ser}	0.7	64	S2BH→195:Nϵ, 2.66, 131 191:NHϵ→HCA, 2.73, 143
	2-2H(H_2)-a	70^{Ile}	0.2	79	S2BH→195:Nϵ, 2.58, 136 191:NHϵ→HCA, 2.92, 144
	2-4H-a	WT	0.3	33	S2BH→195:Nϵ, 2.56, 152 191:NHϵ→HCA, 2.37, 138
	2-4H-a: TS	WT	0.4	34	S2BH→195:Nϵ, 2.55, 152 191:NHϵ→HCA, 2.33, 139
	2-4H-a	69^{Ser}	0	33	S2BH→195:Nϵ, 2.69, 154 191:NHϵ→HCA, 2.88, 130
	2-4H-a	70^{Ile}	1.2	84	S2BH→195:Nϵ, 2.64, 150 191:NHϵ→HCA, 2.45, 118
endo-Fe2-η^1	**2-2H(H_2)-b**	WT	0.5	50	S2BH→195:Nϵ, 3.18, 118 191:NHϵ→HCA, 2.48, 138
	2-2H(H_2)-b: TS	WT	0.5	59	S2BH→195:Nϵ, 3.03, 110 191:NHϵ→HCA, 2.35, 141
	2-2H(H_2)-b	69^{Ser}	0.5	35	S2BH→195:Nϵ, 3.26, 121 191:NHϵ→HCA, 3.02, 135
	2-2H-e	WT	0.5	48	195:Hϵ→S2Be, 2.77, 135 191:NHϵ→HCA, 2.41, 134
	2-2H-e	69^{Ser}	0.9	45	195:Hϵ→S2Bϵ, 2.83, 133 191:NHϵ→HCA, 3.02, 134
exo-Fe2-η^2	**1-1H(H_2)-b**	WT	0.8	62	191:NHϵ→HCA, 1.85, 163

[a] TS = transition state. [b] HCA = atom O1 of homocitrate.

alternative conformations of side-chains, alternative water positions, or alternative hydrogen bonding), and from energy errors in the force field.

The cofactor transplantations into protein involve the wild-type and also experimentally relevant mutant proteins. For the α-$69^{Gly\rightarrow Ser}$ mutant, which retains full N_2 activity, the conformation of the side-chain is not known experimentally, so I have optimized the three possibilities. In all cases, the CH_2OH group is too distant to directly affect coordination at Fe6, but one of the conformers engages hydrogen bonds involving the carbonyl of α-65^{Gly} and water molecule 34, which in turn is hydrogen bonded to a terminal carboxylate (O2) of homocitrate (Figure 8). The concomitant movement of homocitrate weakens the otherwise good hydrogen bond of homocitrate O1 with the side-chain of α-191^{Gln}. This conformer of α-69^{Ser} is the same as that previously described.[13] The phenyl side-chain of α-381^{Phe} lies immediately behind S2B of FeMo-co (Figure 8) and is required to move, mainly backward, when there is endo-

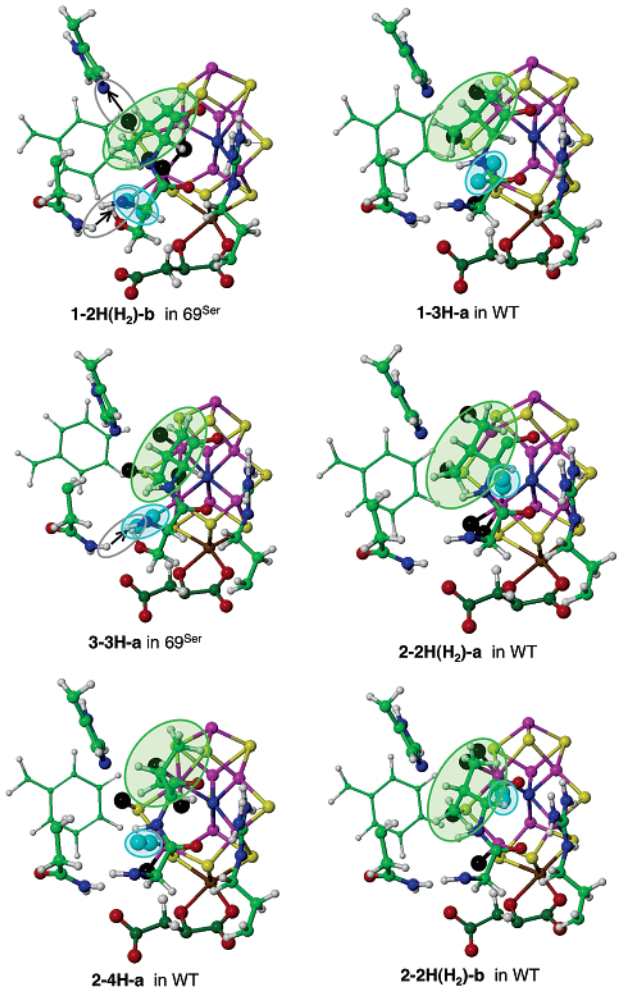

Figure 9. The optimized structures of the transplants of selected models of ligated FeMo-co into the MoFe protein, as wild-type (WT) or α-69^{Ser} mutant. N_2 is cyan; H atoms bound to FeMo-co are black. The standard view direction is the same as that of Figure 8, which identifies the amino acids: α-69 and α-70^{Val} are shown in full, but only the side-chains of α-96^{Arg}, α-191^{Gln}, 195^{His}, and α-381^{Phe} are shown. The lower section of homocitrate (C dark green) is omitted, as are water molecules. Significant hydrogen bonds are marked with arrows and enclosed in gray. N_2 is enclosed in cyan, and the side-chain of α-70^{Val} is emphasized in green.

coordination at either or both of Fe2 and Fe6. In ligated FeMo-co models where S2B is hydrogenated, the resting state hydrogen bond from α-195^{His}:Hϵ to S2B is replaced with a potential hydrogen bond from S2B-H to Nϵ of α-195^{His}, and in the transplant calculations the imidazole group of α-195^{His} is protonated at Nδ rather than Nϵ.

The transplant calculations were made for representative ligated cofactors, involving N_2 coordinated in η^2 and η^1 modes, in endo and exo positions, at Fe6 and Fe2, and transplanted into both the wild-type and the α-69^{Ser} proteins. The results are presented in Table 3, and some are pictured in Figure 9 in the standard view direction (to be compared with Figure 8) with the relative juxtapositions of bound N_2 and the side-chain of α-70^{Val} emphasized with the cyan and green enclosures. Notice that there are small variations in the positions and conformation of the side-chains of α-70^{Val}, α-191^{Gln}, and α-195^{His}, with larger variations in the position of the side-chain of α-381^{Phe}, forced by the backward position of S2B due to endo ligation at Fe2 and/or Fe6. What is not evident in Figure 9 is any movement of α-70^{Val} and its helix in the direction normal to the FeMo-co face: this is assessed via increases in the N^c−70:Cα distance, reported in Table 3, together with dimensions of the possible hydrogen bonds and the estimated protein strain energies. Table 3 also contains the results of transplants into other protein mutants, and transplants of some of the transition states for coordination of N_2. Results for both directions of the possible hydrogen bond between S2B and α-195^{His} are included. In all cases, there is no significant change in α-96^{Arg} and its hydrogen bond with S5A. Also, the side-chain of α-71^{Val}, adjacent to α-70^{Val}, does not contact ligands on FeMo-co.

The CH_2Ph side-chain of α-381^{Phe} is required to move backward and often upward (e.g., **3-3H-a**) or downward (e.g., **2-2H(H$_2$)-a**), by van der Waals repulsion with S2B. This side-chain is contiguous with α-191^{Gln}, and the movements of these groups are loosely coupled. From observation of the protein relaxations after retransplantation of bare FeMo-co, it is estimated that the strain energy associated with movement of α-381^{Phe} is ca. 15 kcal mol^{-1}. Virtually all models at the E_3H_3 and E_4H_4 stages have endo ligands (N_2, H, or H_2) at Fe2 or Fe6 (including those with the common Fe2−H−Fe6 bridge) and require this movement of α-381^{Phe}. Therefore, 15 kcal mol^{-1} should be subtracted from the total strain energy in Table 3 in estimating the strain associated with other changes, particularly in the front helix containing residues α-69 and α-70.

The principal outcomes of the cofactor transplantation calculations, and implications for the coordination of N_2, are summarized in the following paragraphs.

(1) Exo-Coordination of N$_2$. At Fe2, exo-η^1-N_2 has severe interference with α-195^{His}, while exo-η^2-N_2 coordination (in **1-1H(H$_2$)-b**) causes strong displacement of α-70^{Val} and α-195^{His}, totally disrupting any S2B-195^{His} hydrogen bonding, and causing large strain in the WT protein. Therefore, it is considered very unlikely that N_2 will be bound at the exo-Fe2 position. In contrast, at exo-Fe6, both η^1- and η^2-coordination of N_2 do not interfere with or cause movement of α-70^{Val}, or α-69^{Ser}, and in **3-3H-a** there is minimal interference with the mutants α-70^{Ile} and α-381^{Arg}. Passage through the transition state for the exo-Fe6−η^1-N_2 binding of **3-3H-a** involves a 14 kcal mol^{-1} increase in protein strain.

(2) Endo η^2-Coordination of N$_2$. Ligands in the endo position of Fe2 and Fe6 are directed toward residue α-70. Endo η^2-coordination at Fe6 (**1-3H-a**) causes negligible movement of α-70^{Val} and relatively small strain: the transition state for this coordination increases the strain by 12 kcal mol^{-1}. This suggests that η^2-N_2 at endo-Fe6 is mechanistically feasible. This conclusion is supported by the calculated result for the mutant α-70^{Ile} protein (experimentally unreactive with N_2), which interferes with structure **1-3H-a** causing the protein to move away by 0.7 Å, incurring an additional 24 kcal mol^{-1} of protein strain energy.

(3) Endo η^1-Coordination of N$_2$. In these transplants, the distal N of the extended Fe−N−N can partly avoid the side-chain α-70^{Val} by being directed toward the main chain Cα atom (see **2-2H(H$_2$)-a**, **2-2H(H$_2$)-b** in Figure 9) or toward the NH bond of α-70^{Val} (see **2-4H-a** in Figure 9). The strain energies are 35−45 kcal mol^{-1} for α-70^{Val}, but increase to ca. 80 kcal mol^{-1} for α-70^{Ile}: this larger strain in the two α-70^{Ile} transplants (Table 3) is due to distortion of the main chain (with **2-2H-(H$_2$)-a**) or contact between distal N and the side-chain (with

2-4H-a). The transition states for endo η^1-coordination at Fe6 in α-70^{Val} protein involve no additional strain with model **2-4H-a** where N_2 is inclined away from Cα atom of α-70^{Val}, but an additional strain of 25−30 kcal mol^{-1} when N_2 is directed at the Cα atom of α-70^{Val} (model **2-2H(H$_2$)-a**). These findings, together with the result for **2-4H-a** in the α-69^{Ser} mutant (Table 3), indicate that η^1-coordination of N_2 in an endo position at Fe6 (as in **2-4H-a**) is feasible and is consistent with the experimental data.

(4) Hydrogen Ligation. The optimum conformation of the α-70^{Val} side-chain is affected by bound H and or H_2, and in a number of transplants there is close van der Waals contact between these H atoms and the methyl groups of the side-chain: examples are **2-4H-a** (Figure 9), **2-2H(H$_2$)-b** (Figure 9), and **1-1H(H$_2$)-b**. In **1-2H(H$_2$)-b** (Figure 9) and **1-1H(H$_2$)-b**, endo-Fe−H_2 forces α-70^{Val} away from the face (Table 3).

(5) Hydrogen Bonding. The backward movement of S2B caused by ligation of FeMo-co generally diminishes the quality of the hydrogen bond between S2B and the α-195^{His} side-chain. One of the S2B-H transplants shown (**1-2H(H$_2$)-b**) has a good hydrogen bond in the S2B-H→195:Nϵ direction, while **2-1H-(H$_2$)-e** has the best 195:Hϵ→S2B hydrogen bond in the opposite direction (Table 3). When N_2 is coordinated (η^1 or η^2) exo at Fe6, it is hydrogen bonded by the side-chain amide N−Hϵ of α-191^{Gln}: this replaces the normal hydrogen bond from α-191: Hϵ to terminal carboxylate O1 of homocitrate. The position and orientation of this terminus of homocitrate, and of surrounding water molecules, are variable.

Before discussing interpretations of these results, I present my investigations of the alternative models A0 and A1 (Figure 10) for the initial binding of N_2, proposed by Kastner and Blochl.[11] I have optimized these structures and transplanted them into WT protein. In both cases, the terminal S2B-H group conflicts with α-195^{His}. In A0, the imidazole side-chain is pushed aside but retains a tight hydrogen bond (195:Hϵ→S2B), while in the A1 structure the S2B-H group conformed as drawn in Figure 10 overlaps the imidazole ring. A transplantation can be achieved after rotation about the Fe2−S2B bond, but the result has S2B against the face of a displaced α-195^{His} imidazole ring, in a position that is chemically unpropitious.

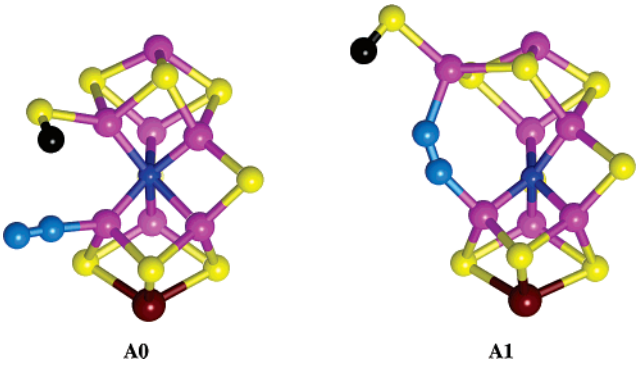

Figure 10. Models proposed by Kastner and Blochl[11] for the early stages of N_2 binding. The additional coordination of Fe1 and Mo, included in the calculations, is not shown.

Discussion and Interpretations

First, the coordination chemistry of FeMo-co allows many possibilities for the binding of N_2, at the exo or endo positions of Fe6 or the endo position of Fe2, with varying degrees and distributions of the hydrogenation representing the E_2H_2, E_3H_3, and E_4H_4 levels of reduction of FeMo-co. However, models with N_2 bridging Fe atoms are unstable to dissociation or rearrangement and are not considered further. Calculations show that similar results and conclusions about the coordination chemistry of FeMo-co with N_2/H/H_2 are expected should the atom at the center of FeMo-co be shown to be C rather than N. Second, the models described generally involve contacts and interactions with the surrounding residues that have been shown in mutation investigations to affect the N_2 activity; there is strong reason to believe that the mechanism of nitrogenase will involve one or more of the models presented here.

An improved procedure is adopted for assessment of the energetic aspects of N_2 coordination, that is calculation of the activation energies for association and dissociation of N_2. These data show considerable variation, primarily according to the η^1 or η^2 coordination mode, secondarily according to the distribution of H atoms and/or H_2 molecules bound to FeMo-co, and are only slightly dependent on whether the coordination is at an exo or endo position of Fe. These comparative association and dissociation barriers will be valuable in the generation and evaluation of hypotheses about subsequent mechanistic steps.

Also introduced in this paper are estimates of the energetic consequences of ligation of FeMo-co by N_2/H/H_2 within its surrounding protein, and in some of the mutant proteins that are relevant experimentally. These calculated protein strain energies provide a further basis for assessment of the various coordination models. In the procedure adopted in this paper, the coordination profiles are calculated independently of the protein movements. However, it would be preferable to have a QM/MM calculation in which the density functional energy gradients for the coordination events are coupled with the force-field gradients for protein movement, but this is a more demanding calculation; the value of the present calculations is that they guide selection of specific systems and mechanistic steps to be treated by QM/MM methods. A caveat is needed for interpretation of the protein strain energies calculated here: they are all relative to bare FeMo-co, which is not the precursor species for the binding of N_2. The contribution of protein strain to the activation energy for the coordination of N_2 should be calculated from the pre-hydrogenated state, and therefore will be less than the energies tabulated; a deconvolution of the energy involved in preparatory movement of α-381^{Phe} is made above. Another caveat is that the accuracy of the calculated protein strain energies is uncertain. The density functional methods used for calculation of the association and dissociation energies have been validated,[13] but the cofactor transplantation methodology (which nevertheless uses the well-developed cvff force-field) has not been directly validated. All of the analysis above is made in terms of internal energies, with neglect of the (unknown but relatively constant) entropy cost when N_2 diffused into the protein is coordinated to Fe, but for the present purposes of identifying and comparing possibilities the variations in internal energies are the primary indicators.

How can the data presented be interpreted to indicate the more probable N_2 binding modes? The response to this question depends on the mechanistic conceptual framework, and the steps to be favorably activated. I envisage the following sequence:

N_2 diffuses toward the Fe2/Fe6 region, aided by externally driven movements of surrounding protein; suitably prehydrogenated FeMo-co[7,13] adjusts to the activation state for N_2 coordination; N_2 associates with Fe6 or Fe2 of FeMo-co; the barrier for dissociation of N_2 should be larger than the barriers for the next steps, which include dissociation of H_2 and the first transfer of an H atom from an S or Fe atom to generate the first intermediate containing N_2H. Calculated reaction profiles for both of these later steps (dissociation of H_2 and H transfer to N_2) are not yet available, but as described in Figure 5 there is one case where coordination of N_2 causes barrierless dissociation of H_2. Preliminary results for the first transfer of H to N_2 indicate that it is likely to have a relatively large activation barrier. In this context, the small barriers for dissociation of η^2-N_2 suggest that this is unlikely to be a competitive coordination mode, because hydrogenation of N_2 would then be uncompetitive with dissociation of N_2. Of the two modes of η^1 cooordination, exo at Fe6 or endo at Fe6 or Fe2, endo coordination engages with residue α-70 and is consistent with the experimental result that α-70^{Ile} is unreactive with N_2: exo-Fe6−η^1-N_2 coordination is not directly consistent with this datum. There is a marginal preference for endo η^1-N_2 coordination at Fe6 over Fe2, on the basis of structure and protein strain. The barriers for the initial association and dissociation of N_2 provide little reason to choose between endo and exo coordination of N_2, and, as already described, the distribution of the hydrogenation is a more important factor.

This all leads to the conclusion that endo-η^1-N_2 coordination at Fe6 is most probable, but any conclusion at this point is tempered by the requirement that the barrier for the next stage, transfer of H to N_2, be surmountable. There is little basis for further speculation now, although the following hypothesis is supportable. N_2 could approach approximately parallel to the face of FeMo-co, in preparatory η^2 geometry requiring minimal displacement and strain for the nearby protein, but then bind to Fe in the η^1 geometry which has greater stabilization. A number of energy minimizations have already shown that an unhooking of η^2 coordination to η^1 coordination geometry has minimal or zero energy barrier.

Do the present results provide insight into and interpretation of the experimental data on mutant proteins? Yes. The unreactivity of α-70^{Ile} with N_2 is proposed to be due simply to steric interference shutting down endo-η^1-N_2 coordination at Fe6 or Fe2. The normal reactivity with N_2 of the α-69^{Ser} mutant is consistent with the lack of contact between N_2 bound at Fe6 (in any mode) and the CH_2OH side-chain. The α-195 mutants are postulated to modify stabilities of the forms of FeMo-co hydrogenated at S2B, but not the binding of N_2 (provided it is at Fe6 or endo at Fe2), which is consistent with the experimental observations that these mutants bind N_2 but do not hydrogenate it. It is postulated that the modifications of α-277 that make it unresponsive to N_2 interfere with the ingress rather than the binding of N_2. At this point, the unreactivity of the α-191^{Lys} mutant is not clearly explained.

Calculated N_2 association/dissociation profiles indicate that the binding of N_2 to more negatively charged FeMo-co is decelerated, with increased association and dissociation barriers. There is no advantage in binding N_2 to FeMo-co between the electronation and protonation events. It is also argued that bound N_2 is not protonated directly from surrounding protein residues or water. The favored model is the accumulation of H atoms on FeMo-co, as previously described,[7,13] followed by N_2 binding, followed by transfer of H to coordinated N_2.

What Next?

The information provided and principles developed here set the stage for the next calculations of possible steps in which H atoms are transferred to bound N_2, and of the probable structures of the intermediates with bound N_2H_x and bound NH_x, prior to release of NH_3. This is in progress.

Attention focuses also on residue α-381. The models developed here require the side-chain of α-381^{Phe} to move from its position in the resting protein to accommodate hydrogenated FeMo-co coordinated with N_2. Because the interaction that causes this is van der Waals repulsion between S2B and the phenyl side-chain, it is not so obvious how this has evolved into an influential interaction in the wild-type enzyme, or what mutations might help uncover this function. A less voluminous side-chain might ease the strain; would it enhance the reactivity with N_2? A hydrogen bonding or proton donor side-chain could engage S2B from behind, changing the dynamics for hydrogenation of S2B, and then the dynamics of N_2 coordination and of H transfer to N_2. In this context, the report[27] that α-381^{Arg} manifests slowed diazotropic growth is significant.

Also needed are investigations of the dynamics of the MoFe protein. Presumably this protein undergoes tertiary and quaternary structural changes, driven in part by its interactions with the Fe protein and changes at the P-cluster associated with electron transfer, to facilitate the ingress and binding of N_2. The calculations reported here represent the response of the protein to coordination events at FeMo-co, but what is needed is the converse, information about the role of the protein in facilitating these events. Crystal structures of the MoFe protein, docked in different ways with the Fe protein, have not revealed conformational changes within the MoFe protein.[28] Calculations using elastic network models[29] could be helpful.

Acknowledgment. This research is supported by the Australian Research Council and the Australian Partnership for Advanced Computing.

Supporting Information Available: Figures S1−3. This material is available free of charge via the Internet at http://pubs.acs.org.

JA0644428

(28) Tezcan, F. A.; Kaiser, J. T.; Mustafi, D.; Walton, M. Y.; Howard, J. B.; Rees, D. C. *Science* **2005**, *309*, 1377−1380.
(29) Atilgan, A. R.; Durell, S. R.; Jernigan, R. L.; Demirel, M. C.; Keskin, O.; Bahar, I. *Biophys. J.* **2001**, *80*, 505−515. Liao, J.-L.; Beratan, D. N. *Biophys. J.* **2004**, *87*, 1369−1377.